Electronic Supplementary Information (ESI)

A decacobalt(II) cluster with triple-sandwich structure obtained by partial reductive hydrolysis of a pentacobalt(II/III) Weakley-type polyoxometalate

Yan Duan,[a] Juan M. Clemente-Juan,[a] José L. G. Fierro,[b] Carlos Giménez-Saiz[a]* and Eugenio Coronado[a]*

[a]Instituto de Ciencia Molecular (ICMol), Universidad de Valencia, c/ Catedrático José Beltrán, 2, 46980 Paterna, Spain.

[b]Instituto de Catálisis y Petroleoquímica, (CSIC), c/Marie Curie, 2, Cantoblanco, 28049 Madrid, Spain.

*E-mail for C. G.-S.: carlos.gimenez@uv.es

*E-mail for E. C.: eugenio.coronado@uv.es

Table of Contents

1. General methods and materials

All reagents were of high purity grade quality, obtained from commercial sources, and used without further purification. Pure water (ρ > 18 MΩ·cm) was used throughout. It was obtained using an Elix-3/Millipore-Q Academic water purification system.

IR spectra were recorded with KBr pellets on a Thermo NICOLET-5700 FT-IR spectrophotometer. Elemental analysis was performed by inductively-coupled-plasma optical-emission-spectroscopy (ICP-OES) on solutions prepared by treating the POMs in a hydrofluoric acid/hydrochloric acid mixture of ratio 1:8 and diluted with water to a known volume. Thermogravimetric analysis was performed on a Metler Toledo TGA/SDTA851e analyzer.

2. Synthesis

Synthesis of $K_{10.5}Na_{0.3}\{Co_{0.6}(H_2O)_{3.6}\}[Co^{II}_4(H_2O)_2(Co^{III}W_9O_{34})(PW_9O_{34})]\cdot 19.4H_2O$ (1a)

$Na_2WO_4\cdot 2H_2O$ (21.60 g, 65.6 mmol) and Na_2HPO_4 (0.84 g, 5.92 mmol) were dissolved in 60 mL of water and the pH of the solution adjusted to 5.5 using glacial acetic acid. Another aqueous solution containing $Co(CH_3COO)_2\cdot 4H_2O$ (5.16 g, 20.72 mmol) in 100 mL of water was added dropwise to the first one, and the pH of the resultant solution was adjusted again to 5.5 using glacial acetic acid. Then, the solution was refluxed for 2 h and hot filtered. To the hot filtrate, potassium acetate (8.96 g, 91.2 mmol) and potassium persulfate (0.44 g, 1.63 mmol) were successively added in small portions. After the addition of the solids, the solution was concentrated at 80 ºC until a final volume of 120 mL was attained. Then, the solution was allowed to cool back to room temperature and a large amount of black precipitate (9.42 g) was formed. This precipitate was recrystallized from the minimum amount of water at 80 ºC to obtain 6.75 g of dark brown prismatic crystals (yield 33%,

based on $Na_2WO_4 \cdot 2H_2O$). IR (2% KBr pellet 1200 – 400 cm^{-1}) (Fig. S4): 1050(m), 1030(s), 937(s), 874(s), 808(w), 738(m, sh), 587(w), 513(m), 425(m, sh). The TGA curve of **1a** (Fig. S5) shows a total weight loss of 8.2% in the range 30 – 800 ºC which agrees with the loss of 25 water molecules (calcd 8.2%). Anal. Calcd (Found) for **1a**: P, 0.55 (0.57); W 58.8 (57.4); Co 5.9 (6.0); K 7.3 (6.9); Na 0.12 (0.15).

Synthesis of $K_6\{Co_9(H_2O)_{42}\}[Co_2\{Co_3(H_2O)(Co(OH)_2W_7O_{26})(PW_9O_{34})\}_2] \cdot 26H_2O$ (2a)

Solid **1a** (0.045 g, 7.9×10^{-3} mmol) was dissolved in 8 mL of water with gentle warming (~65 ºC) under stirring, giving rise to a dark brown solution. Then, 1 mL of hydrazine solution (1.0 M in THF) was added dropwise to the warm solution, causing a gradual color change from dark brown to light violet. After the addition, the solution (pH ~ 7.6) was stirred for 30 min at ~ 65 ºC, filtered with paper and allowed to stand at room temperature in an open vial. Upon standing, an upper, light pink, clear phase and a lower, violet, cloudy phase formed, which were mechanically separated using a Pasteur pipette. The light pink solution was allowed to evaporate further at room temperature during one month until pink, needle-like, crystals were obtained and identified by IR and X-ray single-crystal diffraction as the previously known $K_6[Co(H_2O)_4]_2[H_2W_{12}O_{42}] \cdot 14H_2O$.[1] To the lower, violet suspension, 5 mL of water were added, so a clear, violet solution was obtained (pH ~ 7.4). After one week of evaporation at room temperature in an open vial, violet needle shaped crystals of **2a** were formed, collected by filtration, washed with a small amount of cold water and air-dried (18 mg, 43% based on **1a**). IR (2% KBr pellet 1200 – 400 cm^{-1}) (Fig. S4): 1032(s), 956(m, sh), 937(s), 880(s), 800(w), 719(s), 626(w), 480(m, sh), 415(s). The TGA curve of **2a** (Fig. S6) shows a total weight loss of 12.7% in the range 30 – 800 ºC which agrees with the loss of 70 water molecules and 4 hydroxyls in the structure (calcd

12.7%). Anal. Calcd (Found) for **2a**: P, 0.59 (0.58); W 56.2 (55.5); Co 10.7 (10.5); K 1.5 (1.2); Na 0 (0.012).

3. X-ray crystallography

Suitable crystals of **1a** and **2a** were coated with Paratone N oil, suspended on small fiber loops, and placed in a stream of cooled nitrogen (120 K) on an Oxford Diffraction Supernova diffractometer equipped with a graphite-monochromated Enhance (Mo) X-ray Source (λ = 0.71073 Å). The data collection routines, unit cell refinements, and data processing were carried out using the CrysAlis software package[2] and structure solution and refinement were carried out using SHELXS-86 and SHELXL-97.[3]

All atoms were refined anisotropically in the two crystal structures except some disordered counter cations and water molecules of solvation having partial occupancies. Analytical absorption corrections were performed for both compounds based on face indexations of the single crystals. Hydrogen atoms of water molecules and hydroxyl anions were not included in the models.

The refinement of the crystal structure of **1a** reveals a 4.6% disorder, which is likely due to a 60º rotation of the whole polyoxoanion. This disorder is only evident for the capping $[W_3O_{15}]$ triad of the $[PW_9O_{34}]^{9-}$ moiety and is not revealed in the remaining W atoms belonging to the six-membered belt of the $[B\text{-}PW_9O_{34}]^{9-}$ moiety, because a 60º rotation brings these W atoms almost into coincidence. The disorder is not apparent for the lighter Co or O atoms due to its small extent (4.6%). In addition, **1a** exhibits also disorder in the solvent/cation region (typical in many polyoxometalate structures). For this reason, some crystalline water molecules and counter cations could not be located. The formula, however, reflects the total number of counter cations and crystalline water molecules

(based on elemental analysis and TGA), as they represent the true bulk composition. The crystallographic data for the two structures are summarized in Table S1.

Table S1. Crystallographic Data for $K_{10.5}Na_{0.3}\{Co_{0.6}(H_2O)_{3.6}\}[Co^{II}_4(H_2O)_2(Co^{III}W_9O_{34})(PW_9O_{34})]\cdot 19.4H_2O$ (**1a**), and $K_6\{Co_9(H_2O)_{42}\}[Co_2\{Co_3(H_2O)(Co(OH)_2W_7O_{26})(PW_9O_{34})\}_2]\cdot 26H_2O$ (**2a**).

Compound	**1a**	**2a**
empirical formula	$Co_{5.6}H_{50}K_{10.5}Na_{0.3}O_{93}PW_{18}$	$Co_{19}H_{144}K_4O_{194}P_2W_{32}$
formula weight	5626.13	10470.36
space group	$P\bar{1}$	*C* 2/m
a/Å	12.2699(3)	30.4947(10)
b/Å	12.3247(2)	14.6754(5)
c/Å	16.6885(4)	23.0718(9)
α/°	89.4877(18)	90
β/°	74.8746(19)	100.584(4)
γ°	60.732(2)	90
V/Å^3	2104.05(8)	10149.5(6)
Z	1	2
T/K	120(2)	120.00(10)
λ/Å	0.71073	0.71073
ρ_{calcd}/g cm^{-3}	4.440	3.426
μ/mm^{-1}	26.225	19.761
$R[F_o^2 > 2\sigma(F_o^2)]$[a]	0.0513	0.0551
$R_w[F_o^2 > 2\sigma(F_o^2)]$[b]	0.1377[c]	0.1383[d]

[a] $R = \Sigma(||F_o| - |F_c||)/\Sigma|F_o|$. [b] $R_w = \{\Sigma[w(F_o^2 - F_c^2)^2]/\Sigma[w(F_o^2)^2]\}^{1/2}$. $w = 1/[\sigma^2(F_o^2) + (AP)^2 + BP]$, where $P = (F_o^2 + 2F_c^2)/3$. [c] $A = 0.0549$, $B = 72.8367$. [d] $A = 0.0643$, $B = 917.7090$.

Table S2. Comparison of the tetrahedral P^V-O, Co^{II}-O or Co^{III}-O bond distances in **1**,[a] **2**,[b] and selected compounds from the literature: $[Co_4(H_2O)_2(PW_9O_{34})_2]^{10-}$,[c] $[Co^{II}W_{12}O_{40}]^{6-}$,[d] and $[Co^{III}W_{12}O_{40}]^{5-}$.[e]

P^V/Co^{III}-O[a]	Co^{II}-O[b]	P^V-O[c]	Co^{II}-O[d]	Co^{III}-O[e]
1.636(13)	1.950(7)	1.528(17)	1.931(14)	1.836(10)
1.700(13)	1.950(7)	1.532(12)	1.931(14)	1.836(10)
1.716(14)	1.953(11)	1.547(14)	1.931(14)	1.836(10)
1.729(14)	1.964(10)	1.552(13)	1.931(14)	1.836(10)

[a] **1** (this work, T = 120 K). P^V and Co^{III} occupy the same crystallographic position inside the tetrahedral cavity of **1** (refined occupancy ca. 50%). [b] **2** (this work, T = 120 K). [c] $[Co_4(H_2O)_2(PW_9O_{34})_2]^{10-}$ (T = 172 K).[4] [d] $[Co^{II}W_{12}O_{40}]^{6-}$ (T = 298 K).[5] [e] $[Co^{III}W_{12}O_{40}]^{5-}$ (T = 298 K).[5]

Table S3. Selected Co-O Bond Distances (Å) and O-Co-O Angles (º) involved in **1** (see Fig. S2 for the labelling of the relevant atoms).

Co(1)-O(1)	1.636(13)	Co(2)-O(1)	2.153(13)
Co(1)-O(2)	1.700(13)	Co(2)-O(10)^i	2.020(11)
Co(1)-O(4)	1.716(14)	Co(2)-O(7)	2.030(12)
Co(1)-O(3)	1.729(14)	Co(2)-O(8)	2.111(12)
Co(2)-O(9)^i	2.114(12)	Co(3)-O(6)	2.052(11)
Co(2)-O(1)^i	2.144(12)	Co(3)-O(8)^i	2.122(11)
Co(3)-O(1)	2.127(12)	Co(3)-O(1W)	2.116(14)
Co(3)-O(5)	2.035(11)	Co(3)-O(9)^i	2.127(11)
O(1)-Co(1)-O(2)	115.6(6)	O(10)^i-Co(2)-O(9)^i	93.1(5)
O(1)-Co(1)-O(4)	112.1(6)	O(7)-Co(2)-O(9)^i	93.8(5)
O(2)-Co(1)-O(4)	106.4(6)	O(8)-Co(2)-O(9)^i	170.7(5)
O(1)-Co(1)-O(3)	111.5(6)	O(10)^i-Co(2)-O(1)^i	91.1(5)

O(2)-Co(1)-O(3)	105.6(6)	O(7)-Co(2)-O(1)^{i}	173.7(5)
O(4)-Co(1)-O(3)	104.9(6)	O(8)-Co(2)-O(1)^{i}	84.3(5)
O(10)^{i}-Co(2)-O(7)	94.6(4)	O(9)^{i}-Co(2)-O(1)^{i}	88.6(5)
O(10)^{i}-Co(2)-O(8)	93.0(4)	O(10)^{i}-Co(2)-O(1)	173.1(5)
O(7)-Co(2)-O(8)	92.7(5)	O(7)-Co(2)-O(1)	91.9(5)
O(8)-Co(2)-O(1)	88.8(4)	O(5)-Co(3)-O(1)	89.8(5)
O(9)^{i}-Co(2)-O(1)	84.4(4)	O(6)-Co(3)-O(1)	90.6(5)
O(1)^{i}-Co(2)-O(1)	82.5(5)	O(8)^{i}-Co(3)-O(1)	84.4(5)
O(5)-Co(3)-O(6)	90.3(5)	O(1W)-Co(3)-O(1)	177.6(6)
O(5)-Co(3)-O(8)^{i}	91.4(4)	O(5)-Co(3)-O(9)^{i}	173.9(5)
O(6)-Co(3)-O(8)^{i}	174.7(5)	O(6)-Co(3)-O(9)^{i}	92.2(5)
O(5)-Co(3)-O(1W)	88.5(6)	O(8)^{i}-Co(3)-O(9)^{i}	85.6(4)
O(6)-Co(3)-O(1W)	91.2(5)	O(1W)-Co(3)-O(9)^{i}	96.9(6)
O(8)^{i}-Co(3)-O(1W)	93.9(5)	O(1)-Co(3)-O(9)^{i}	84.7(5)

Symmetry transformations: (*i*) –x+2, –y+1, –z.

Table S4. Selected Co-O Bond Distances (Å) and O-Co-O Angles (º) involved in **2** (see Fig. S3 for the labelling of the relevant atoms).

Co(1)-O(3C)	2.025(9)	Co(2)-O(1P)	2.261(8)
Co(1)-O(3C)^{i}	2.025(9)	Co(3)-O(678)^{i}	1.946(8)
Co(1)-O(1W)	2.103(14)	Co(3)-O(678)	1.946(8)
Co(1)-O(6C)^{i}	2.115(8)	Co(3)-O(2H)	1.951(12)
Co(1)-O(6C)	2.115(8)	Co(3)-O(1H)	1.972(11)
Co(1)-O(1P)	2.227(11)	Co(4)-O(74C)^{ii}	2.073(8)
Co(2)-O(4C)	2.003(9)	Co(4)-O(74C)	2.073(8)
Co(2)-O(73C)	2.041(8)	Co(4)-O(8C)	2.089(8)
Co(2)-O(5C)	2.046(9)	Co(4)-O(8C)^{ii}	2.089(8)
Co(2)-O(1H)	2.064(7)	Co(4)-O(2H)^{iii}	2.109(8)
Co(2)-O(6C)	2.104(8)	Co(4)-O(2H)	2.109(8)
O(3C)-Co(1)-O(3C)^{i}	87.4(5)	O(73C)-Co(2)-O(1P)	174.4(3)
O(3C)-Co(1)-O(1W)	89.3(4)	O(5C)-Co(2)-O(1P)	90.8(4)
O(3C)^{i}-Co(1)-O(1W)	89.3(4)	O(1H)-Co(2)-O(1P)	80.7(3)
O(3C)-Co(1)-O(6C)^{i}	174.2(4)	O(6C)-Co(2)-O(1P)	83.2(4)
O(3C)^{i}-Co(1)-O(6C)^{i}	93.0(3)	O(678)^{i}-Co(3)-O(678)	114.9(5)
O(1W)-Co(1)-O(6C)^{i}	96.5(4)	O(678)^{i}-Co(3)-O(2H)	108.1(3)
O(3C)-Co(1)-O(6C)	93.0(3)	O(678)-Co(3)-O(2H)	108.1(3)
O(3C)^{i}-Co(1)-O(6C)	174.2(4)	O(678)^{i}-Co(3)-O(1H)	109.4(3)
O(1W)-Co(1)-O(6C)	96.5(4)	O(678)-Co(3)-O(1H)	109.4(3)
O(6C)^{i}-Co(1)-O(6C)	85.9(4)	O(2H)-Co(3)-O(1H)	106.6(5)
O(3C)-Co(1)-O(1P)	90.4(3)	O(74C)^{ii}-Co(4)-O(74C)	91.4(5)

O(3C)^{i}-Co(1)-O(1P)	90.4(3)	O(74C)^{ii}-Co(4)-O(8C)	92.7(3)
O(1W)-Co(1)-O(1P)	179.5(5)	O(74C)-Co(4)-O(8C)	87.7(3)
O(6C)^{i}-Co(1)-O(1P)	83.8(3)	O(74C)^{ii}-Co(4)-O(8C)^{ii}	87.7(3)
O(6C)-Co(1)-O(1P)	83.8(3)	O(74C)-Co(4)-O(8C)^{ii}	92.7(3)
O(4C)-Co(2)-O(73C)	94.2(4)	O(8C)-Co(4)-O(8C)^{ii}	179.5(4)
O(4C)-Co(2)-O(5C)	86.7(4)	O(74C)^{ii}-Co(4)-O(2H)^{iii}	94.6(3)
O(73C)-Co(2)-O(5C)	92.8(4)	O(74C)-Co(4)-O(2H)^{iii}	170.8(4)
O(4C)-Co(2)-O(1H)	169.2(4)	O(8C)-Co(4)-O(2H)^{iii}	85.1(4)
O(73C)-Co(2)-O(1H)	95.1(3)	O(8C)^{ii}-Co(4)-O(2H)^{iii}	94.5(4)
O(5C)-Co(2)-O(1H)	87.5(4)	O(74C)^{ii}-Co(4)-O(2H)	170.8(4)
O(4C)-Co(2)-O(6C)	94.0(3)	O(74C)-Co(4)-O(2H)	94.6(3)
O(73C)-Co(2)-O(6C)	93.1(3)	O(8C)-Co(4)-O(2H)	94.5(4)
O(5C)-Co(2)-O(6C)	174.0(4)	O(8C)^{ii}-Co(4)-O(2H)	85.1(4)
O(1H)-Co(2)-O(6C)	90.9(4)	O(2H)^{iii}-Co(4)-O(2H)	80.4(5)
O(4C)-Co(2)-O(1P)	90.2(3)		

Symmetry transformations: (*i*) x, –y+1, z; (*ii*) –x, y, –z and (*iii*) –x, –y+1, –z.

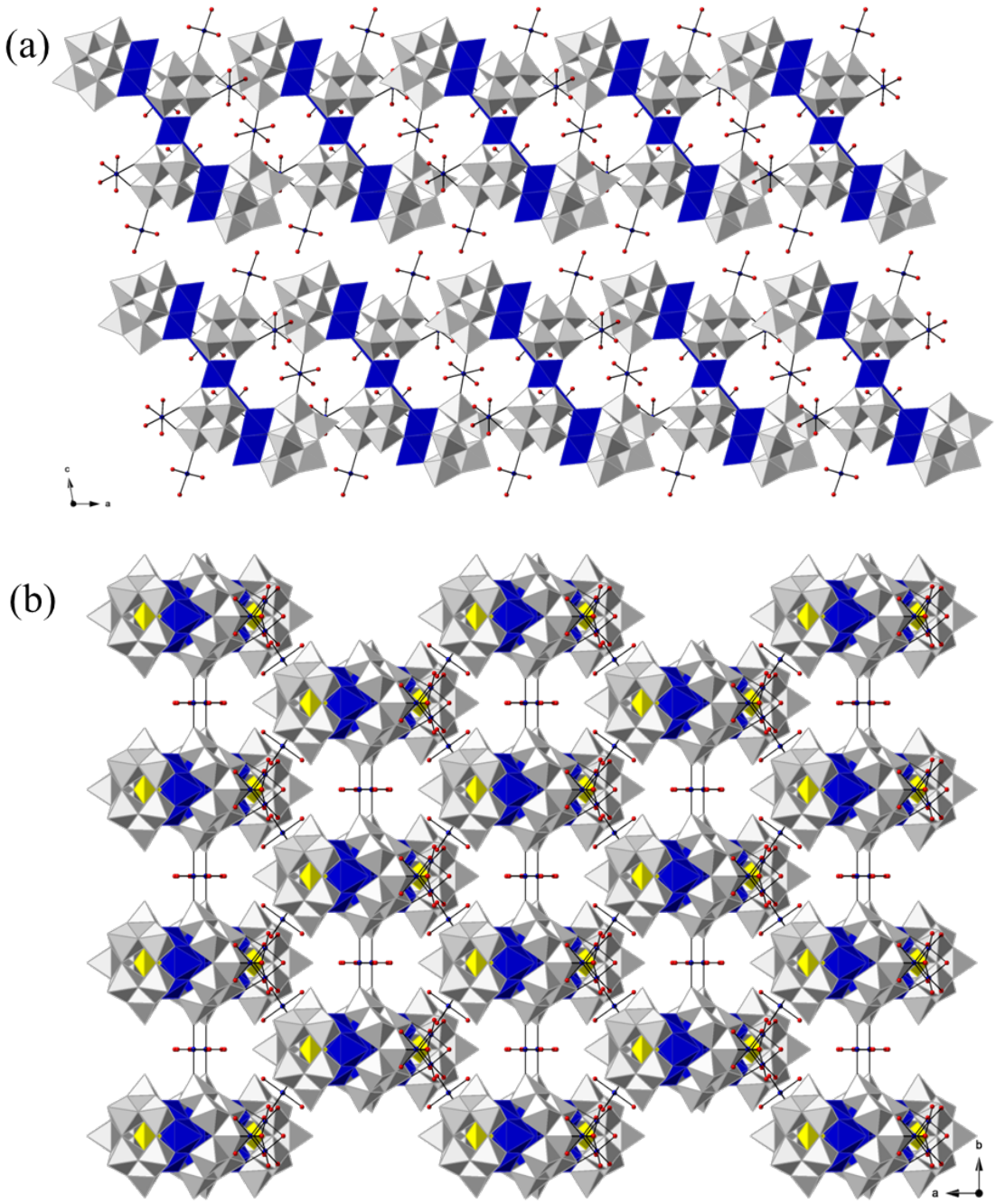

Fig. S1. Polyhedral and ball-and-stick representations for **2a**. (a) Packing mode of $[Co_2\{Co_3(H_2O)(Co(OH)_2W_7O_{26})(PW_9O_{34})\}_2]^{22-}$ layers along *b*-axis. (b) The 2-D sheet architecture constructed from $[Co_2\{Co_3(H_2O)(Co(OH)_2W_7O_{26})(PW_9O_{34})\}_2]^{22-}$ and Co^{II} linkers along *c*-axis in **2a**. Lattice cations and water molecules are omitted for clarity.

4. Bond valence sum (BVS) calculations

The determination of the oxidation states of metal centers and the protonation states of oxygen sites, bond valence sum (BVS) calculations were carried out using the method of I. D. Brown.[6] The calculation formula is $S_i = \exp[(R_0 - R_i)/B]$, where S_i is the bond valence of bond *i*, R_0 is a constant dependent upon the bonded elements, R_i is the bond length of bond *i*, and B equals to 0.37. R_0 values were taken from the literature for calculations performed on cobalt[7] and oxygen[7,8] sites [R_0 (Co–O) = 1.67].

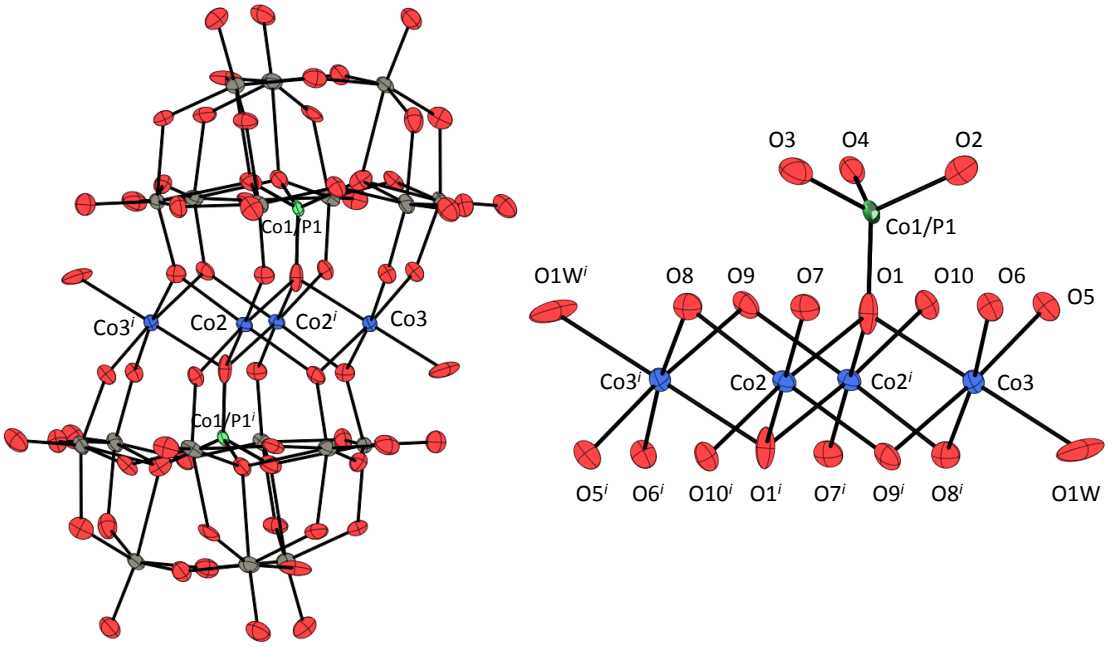

Fig. S2. Thermal ellipsoid plot and numbering scheme for polyoxoanion **1** (50% probability). Symmetry transformations: (*i*) –x+2, –y+1, –z.

Table. S5. Bond valence sum (BVS) calculations for cobalt centres and relevant oxygen sites of **1**.

Cobalt atoms	BVS
Co1/P1	ǂ
Co2	**1.90**
Co3	**1.93**

Oxygen atoms	BVS	Assigned protonation levels
O1	#	-
O2	#	-
O3	#	-
O4	#	-
O1W	**0.30**	**H_2O**
O5	**1.76**	**O**
O6	**1.82**	**O**
O7	**1.83**	**O**
O8	**1.89**	**O**
O9	**1.91**	**O**
O10	**1.75**	**O**
O11	**1.66**	**O**
O12	**1.84**	**O**
O13	**1.69**	**O**
O15	**1.75**	**O**
O17	**1.67**	**O**
O19	**1.64**	**O**
O21	**1.69**	**O**
O32	**1.78**	**O**
O33	**1.63**	**O**
O34	**1.74**	**O**

ǂ This atomic position is occupied by cobalt (Co1) and phosphorous (P1) (50% / 50%), so the bond distances are not adequate to perform BVS calculations.

These oxygen atoms are bonded to the disordered Co1/P1 position. Therefore the BVS calculations have not been performed for these oxygen atoms, although, reasonably they should not be protonated, as they are internal O atoms of **1**.

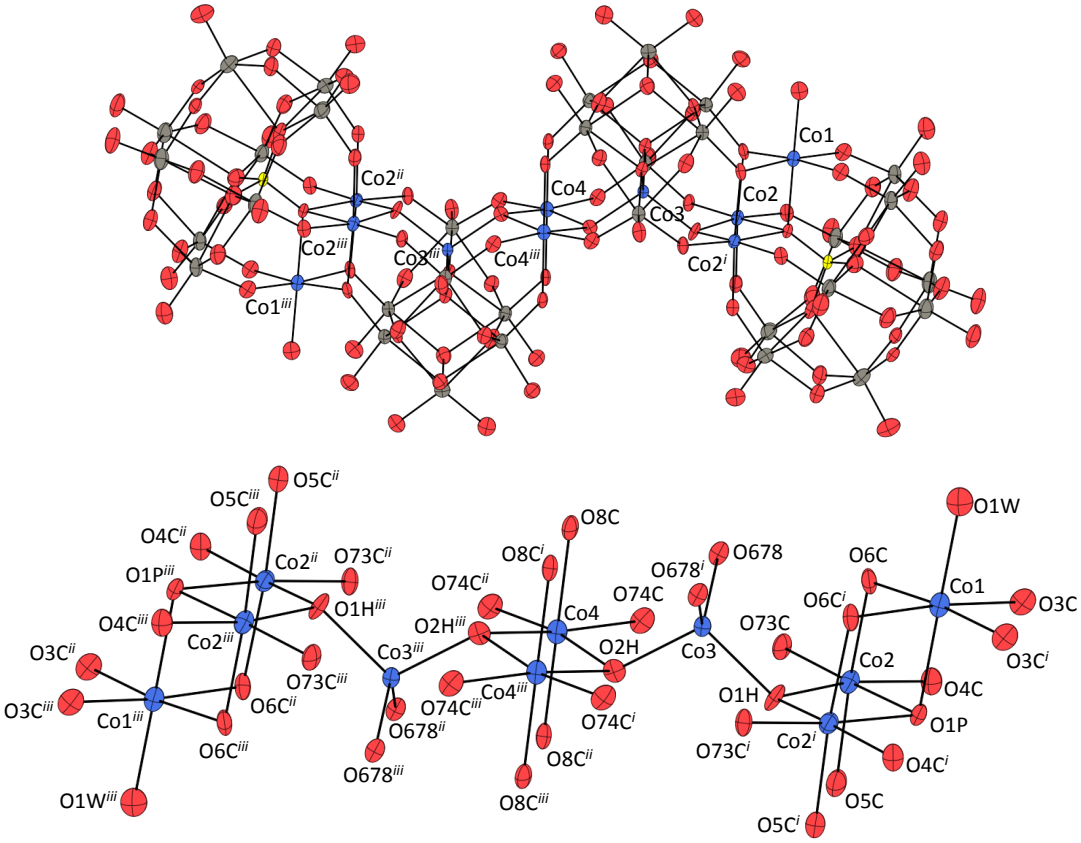

Fig. S3. Thermal ellipsoid plot and numbering scheme for polyoxoanion **2** (50% probability). Symmetry transformations: (*i*) x, –y+1, z; (*ii*) –x, y, –z and (*iii*) –x, –y+1, –z.

Table. S6. Bond valence sum (BVS) calculations for cobalt centres and relevant oxygen sites of **2**.

Cobalt atoms	BVS
Co1	**1.90**
Co2	**1.98**
Co3	**1.85**
Co4	**1.93**

Oxygen atoms	BVS	Assigned protonation levels
O1H	**1.14**	**OH**
O2H	**1.08**	**OH**
O1W	**0.31**	**H_2O**
O1P	**1.80**	**O**
O3C	**1.87**	**O**
O4C	**1.89**	**O**
O5C	**1.86**	**O**
O6C	**1.94**	**O**
O73C	**1.77**	**O**
O74C	**1.77**	**O**
O8C	**1.91**	**O**
O678	**1.98**	**O**
O9A	**1.69**	**O**
O9B	**1.61**	**O**

5. IR spectra

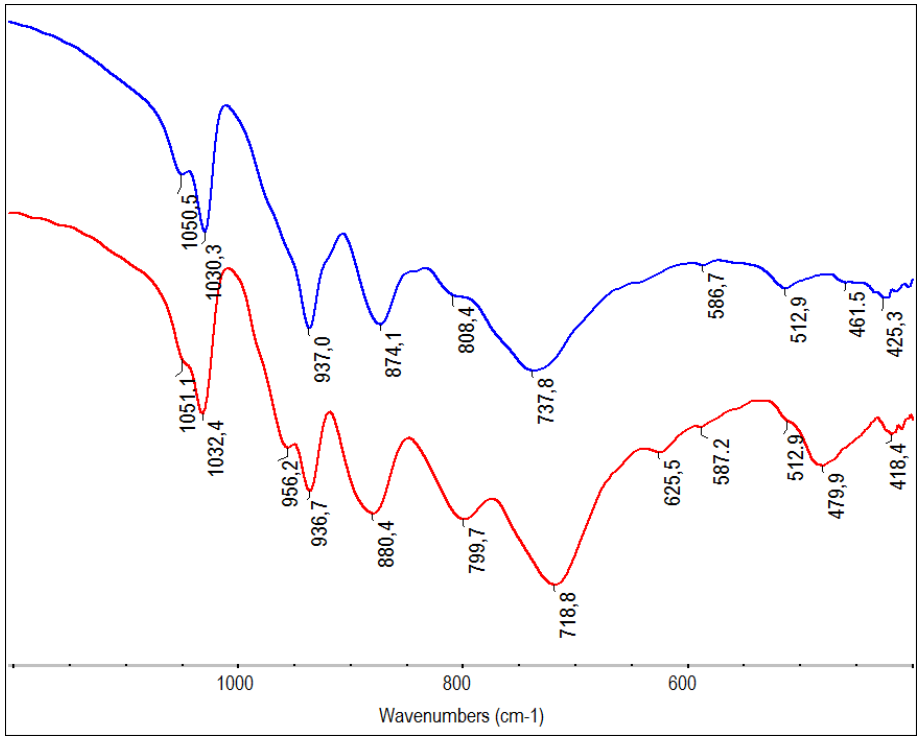

Fig. S4. FT-IR spectra of **1a** (blue) and **2a** (red).

6. Thermogravimetric analysis

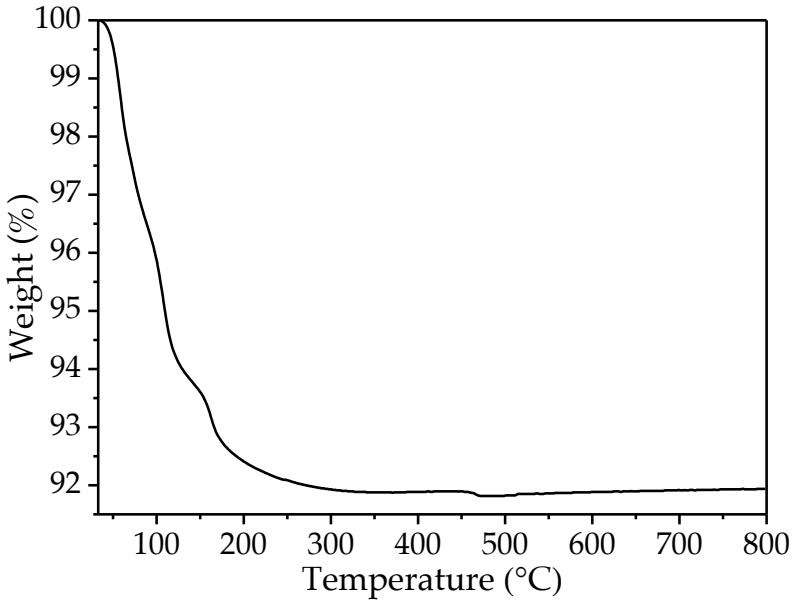

Fig. S5. Thermogram of **1a** from room temperature to 800 ºC (experimental total weight loss 8.2%).

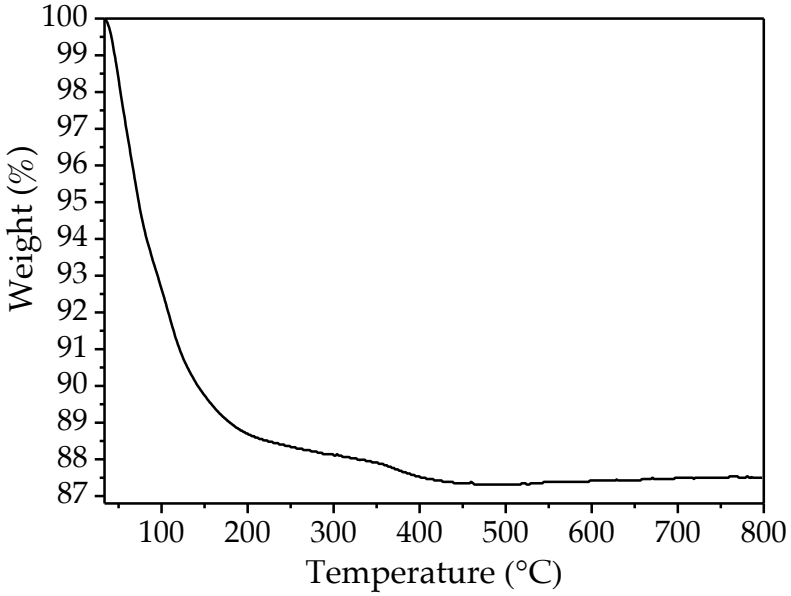

Fig. S6. Thermogram of **2a** from room temperature to 800 ºC (experimental total weight loss 12.7%).

7. X-ray powder diffraction

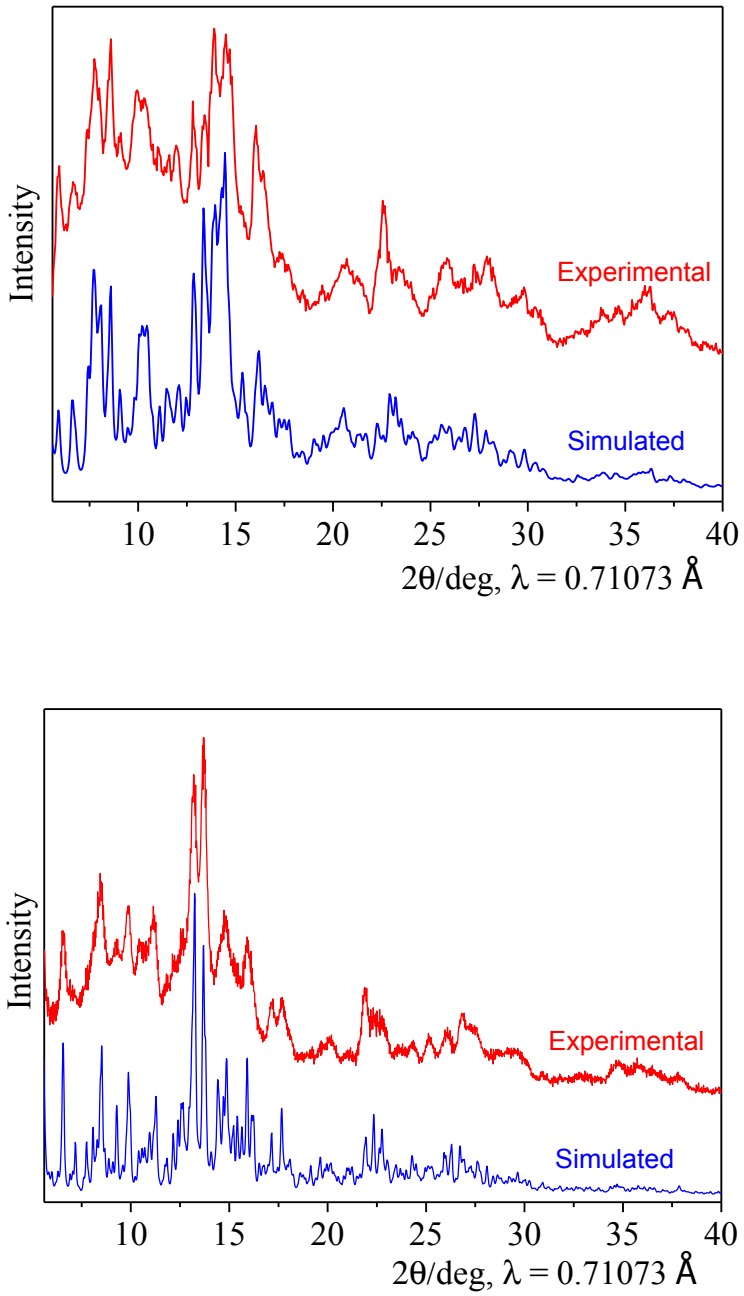

Fig. S7. Comparison of simulated and experimental powder X-ray diffraction patterns for **1a** (up) and **2a** (down). The experimental powder X-ray diffraction pattern was obtained from powdered samples in an *Oxford Diffraction Supernova* diffractometer. The simulated pattern was generated from the atomic coordinates of the single-crystal structure solution using the program Mercury 3.0 (copyright CCDC, http://www.ccdc.cam.ac.uk/mercury/) and a FWHM (full width at half maximum) of 0.2.

8. UV-visible spectroscopy

The UV-vis spectra of the relevant POM were recorded on an Agilent 8453 UV-vis spectrophotometer from 190 to 700 nm using 1.000-cm-optical-path quartz cuvettes in unbuffered water solution and also in 0.5 M NaOAc/HOAc buffered solution at pH 4.8.

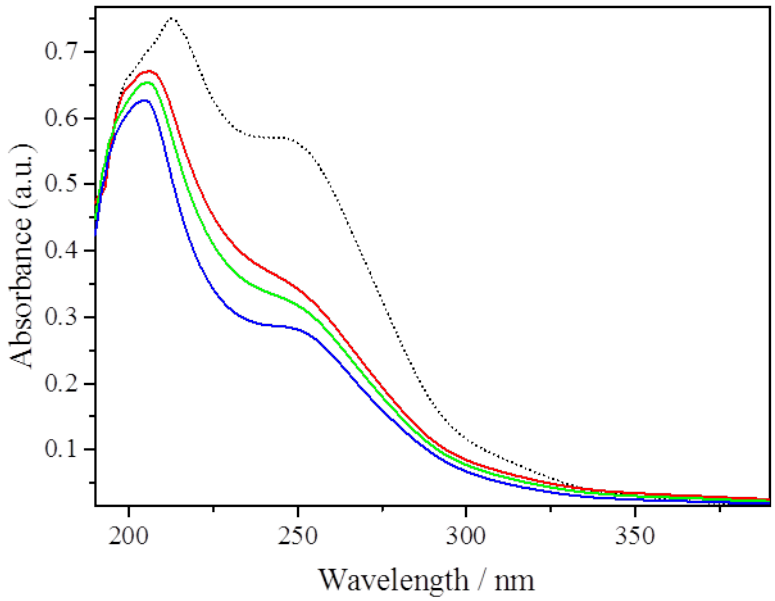

Fig. S8. UV spectrum of an aqueous solution of $[Co^{II}_4(H_2O)_2(PW_9O_{34})_2]^{10-}$ (2×10^{-5} M) (black dotted line). UV spectrum of a solution of **1a** (2×10^{-5} M) in a fresh aqueous solution (red line). UV spectra of the same solution after 15 days (green line), and after 30 days (blue line).

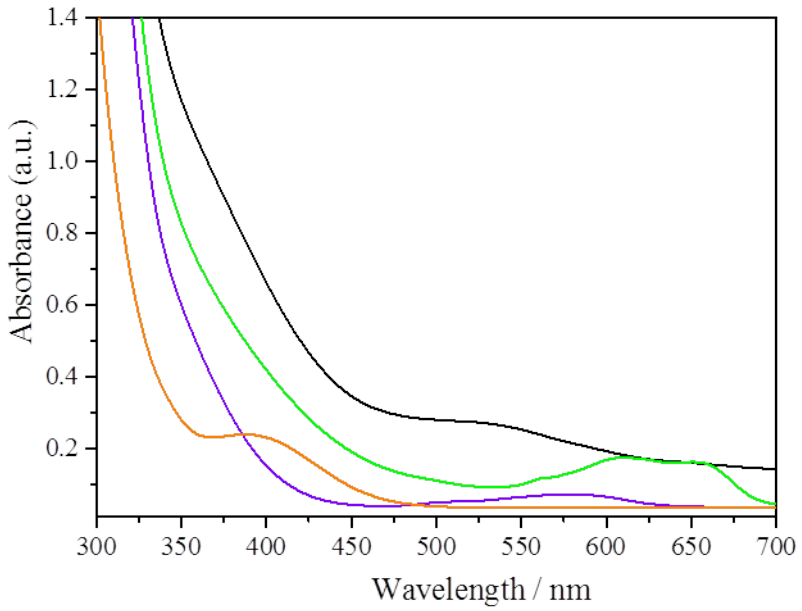

Fig. S9. Visible spectra of **1a** (2×10^{-5} M) (black line), $[Co^{II}_4(H_2O)_2(PW_9O_{34})_2]^{10-}$ (2×10^{-5} M) (violet line), $[Co^{III}W_{12}O_{40}]^{5-}$ (2×10^{-5} M) (orange line) and $[Co^{II}_3W(H_2O)_2(Co^{II}W_9O_{34})_2]^{12-}$ (2×10^{-5} M) (green line) in 0.5 M NaOAc/HOAc buffered solution at pH 4.8.

9. Mass spectroscopy

Electrospray ionization mass spectrometry was performed on a Q-TOF Premier mass spectrometer with an orthogonal Z-spray electrospray source (Waters, Manchester, UK). The temperature of the source block was set to 100 °C and the desolvation temperature to 200°C. A capillary voltage of 3.3 kV was used in the negative scan mode and the cone voltage was set to Uc = 10 V to control the extent of fragmentation of the identified species). Aqueous sample solutions of compound **1a** (ca. 1×10^{-5} M) were infused via a syringe pump, directly connected to the ESI source, at a flow rate of 10 $\mu L \cdot min^{-1}$.

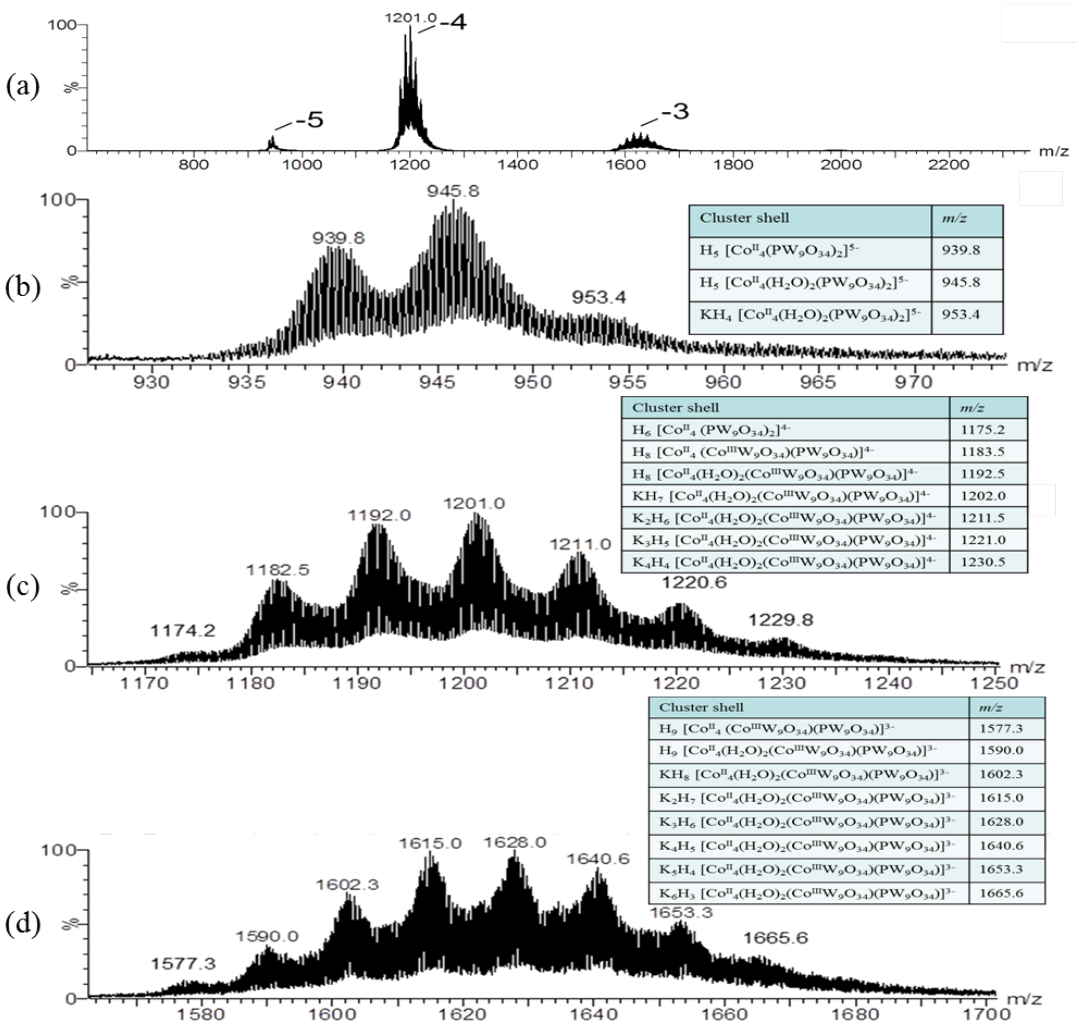

Fig. S10. (a) Mass spectrum (ESI-MS) in negative mode of **1a** in the *m/z* range of 600–2400 in unbuffered water solution. (b) Expanded view of the −5 charge state (*m/z* range 920–980). (c) Expanded view of the −4 charge state (*m/z* range 1160–1250). (d) Expanded view of the −3 charge state (*m/z* range 1560–1700).

The negative-mode electrospray-ionization mass spectrometry of **1a** in unbuffered aqueous solution shows three series of signals (Fig. S10a). At the *m/z* range of 1560-1700, the observed distribution envelopes could be assigned exclusively to **1**, with the formula $[Co^{II}_4(H_2O)_2(Co^{III}W_9O_{34})(PW_9O_{34})]^{12-}$ (with or without the coordinated water molecules). The peaks in the region *m/z* 1160–1250 could be assigned mainly to **1** (either with or

without coordinated water molecules, as before), with only the minor peak located at *m/z* = 1174.2 being assigned to the previously known $[Co^{II}_4(H_2O)_2(PW_9O_{34})_2]^{10-}$ (without the coordinated water molecules). Finally, the minor peaks in the *m/z* range 920-980 correspond to the $[Co^{II}_4(H_2O)_2(PW_9O_{34})_2]^{10-}$ POM (either with or without coordinated water molecules). The occasional loss of the coordinated water molecules is due to the experimental conditions used during the ionization process of the species in the gas phase. These results support the partial decomposition of **1** into POM $[Co^{II}_4(H_2O)_2(PW_9O_{34})_2]^{10-}$ in aqueous solution (with the dominant species being **1**, $[Co^{II}_4(H_2O)_2(Co^{III}W_9O_{34})(PW_9O_{34})]^{12-}$), as previously shown by UV-vis spectroscopy (see Fig. S8).

10. Magnetic properties

Samples of **1a** and **2a** were prepared by compacted powder molded from ground crystalline samples. Each sample was covered with the minimum amount of liquid eicosane (40ºC) in order to prevent crystallite torquering. Variable-temperature susceptibility measurements were carried out in the temperature range 2-300 K on a magnetometer equipped with a SQUID sensor (Quantum Design MPMS-XL-5). The data were corrected for diamagnetic contribution from eicosane and for the diamagnetic contributions of the polyanions, as deduced by using the Pascal's constant tables. Isothermal magnetization measurements at low temperature (2 K and 5 K) were performed up to a field of 5 T in the same apparatus.

Regarding compound **2a**, the ferromagnetic sign of the exchange parameters for edge-sharing CoO_6 octahedra can be associated with the orthogonality of the magnetic orbitals, Co–O–Co angles being close to 90°. The validity of the exchange model and fit is

confirmed by the magnitude of the obtained exchange parameters, which is in good agreement with analogous, previously published, edge-sharing oxo-cobalt clusters encapsulated by POMs.[9] Antiferromagnetic interaction between tetrahedral and octahedral cobalts was expected due to Co–O–Co angles far from 90°. The energy level scheme results from a competition between ferro and antiferromagnetic interactions, leading to a diamagnetic ground state with a S = 1 excited state at 2 cm^{-1}.

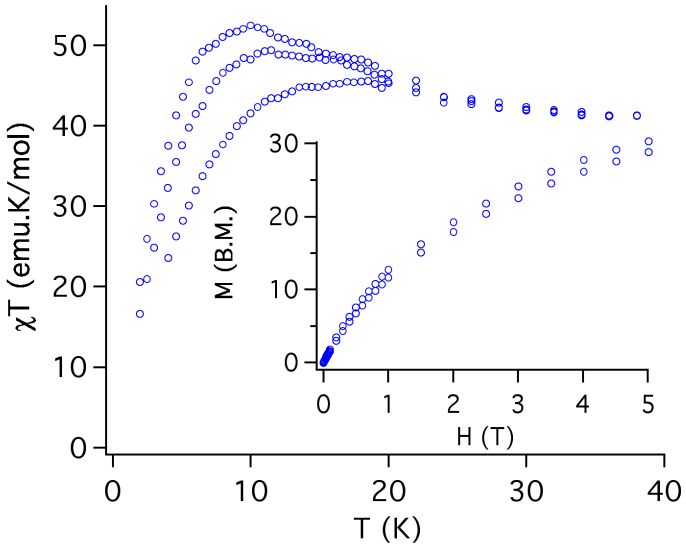

Fig. S11. Thermal behavior of χT for **2a** at different fields (0.5, 1, and 2.5 T) in the range 2 – 40 K. Inset: Magnetization of the same sample at 2 and 5 K in the range 0 – 5 T.

AC susceptibility measurements were also performed for **1a** with an ac field amplitude of 3 Oe and in the absence of dc field. The in-phase and out-of-phase ac susceptibilities are shown in Fig. S12. **1a** doesn't show an out-of-phase magnetic susceptibility. This is not strange even if the tetrahedral Co^{III} has a large negative zero-field splitting, because this cobalt is coupled anti-ferromagnetically with other four octahedral Co^{II}. Therefore, the large anisotropy of isolated cobalt does not directly indicate a large anisotropic ground state of the couples system, in fact in this case the ground state is mainly diamagnetic, S = 0.

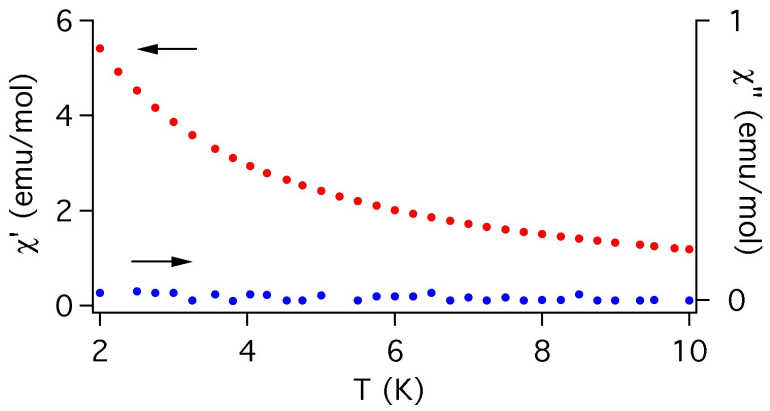

Fig. S12. In-phase (red) and Out-of-phase (blue) ac susceptibility of **1a** in the range 2 – 10 K.

11. X-ray photoelectron spectroscopy

X-ray photoelectron spectra were recorded with a VG 200R spectrometer equipped with a hemispherical electron analyzer and an Al Kα (hν = 1486.6.6 eV) X-ray source. The X-ray source operated at 10 keV and 10 mA. Survey and high-resolution spectra were collected at 65° to the detector with pass energy resolutions of 200 and 50 eV, respectively. The linearity of the binding energy scale was calibrated against the Au $4f_{7/2}$ (84.0 eV) and the Cu $2p_{3/2}$ (932.6 eV) photoemission lines by standard procedures. Each sample was first placed in an aluminum holder mounted on a sample-rod placed in the pre-treatment chamber of the spectrometer and then it was degassed at ambient temperature for 1 hour before being transferred to the analysis chamber. Residual pressure within the ion-pumped analysis chamber was kept below 7×10^{-9} mbar during data acquisition. Binding energies were calculated with respect to the C-(C, H) component of the C1s peak fixed at 284.8 eV. The high resolution spectra for the regions of interest were curve fitted using XPS Peak software. After subtraction of a Shirley background, the peaks were fitted using a nonlinear, least squares routine with mixed Gauss–Lorentz (90/10) functions. A minimum set of

Gauss–Lorentz functions was chosen in order to obtain a reasonable fit.

It is possible to distinguish Co oxidation states using photoelectron spectroscopy. Although the binding energies alone of Co2p lines in compounds containing Co^{II} and Co^{III} ions do not allow unambiguously to discriminate between them, it is feasible when looking at the satellite lines which accompany the principal Co2p ones. We have carried out X-ray photoelectron spectroscopy measurements of **1a** and two other known POMs: $K_6[Co^{II}W_{12}O_{40}]$ and $K_5[Co^{III}W_{12}O_{40}]$, which contain tetrahedrally coordinated Co^{II} and Co^{III}, respectively. Co2p core-level spectra of the three samples are displayed in Fig. S13 and the corresponding binding energies of the most intense peak of the doublet ($Co2p_{3/2}$) are collected in Table S7. All samples show intense satellite structures on the high binding-energy side of the main lines indicating that a certain proportions of Co^{II} are presented in all samples. The relative Co^{II}/Co^{III} ratios in these samples can be estimated by looking at the satellite/Co2p ratios (red values shown in Table S7). These values indicate that the proportion of Co^{III} ions increases in the samples following the order $K_6[Co^{II}W_{12}O_{40}]$, **1a** and $K_5[Co^{III}W_{12}O_{40}]$, as expected. This result demonstrates the presence of Co^{III} ions in solid samples of **1a**.

Table S7. Binding energies (eV) of core-levels of Co-containing samples: $K_6[Co^{II}W_{12}O_{40}]$, $K_5[Co^{III}W_{12}O_{40}]$ and **1a**. The red values correspond to the ratio between the satellite line and the overall $Co2p_{3/2}$ line (satellite included).

	$W4f_{7/2}$	$Co2p_{3/2}$	O1s
$K_6[Co^{II}W_{12}O_{40}]$	35.0	779.8 (0.436)	530.1
$K_5[Co^{III}W_{12}O_{40}]$	34.8	781.2 (0.341)	529.9
1a	35.4	781.2 (0.393)	530.3

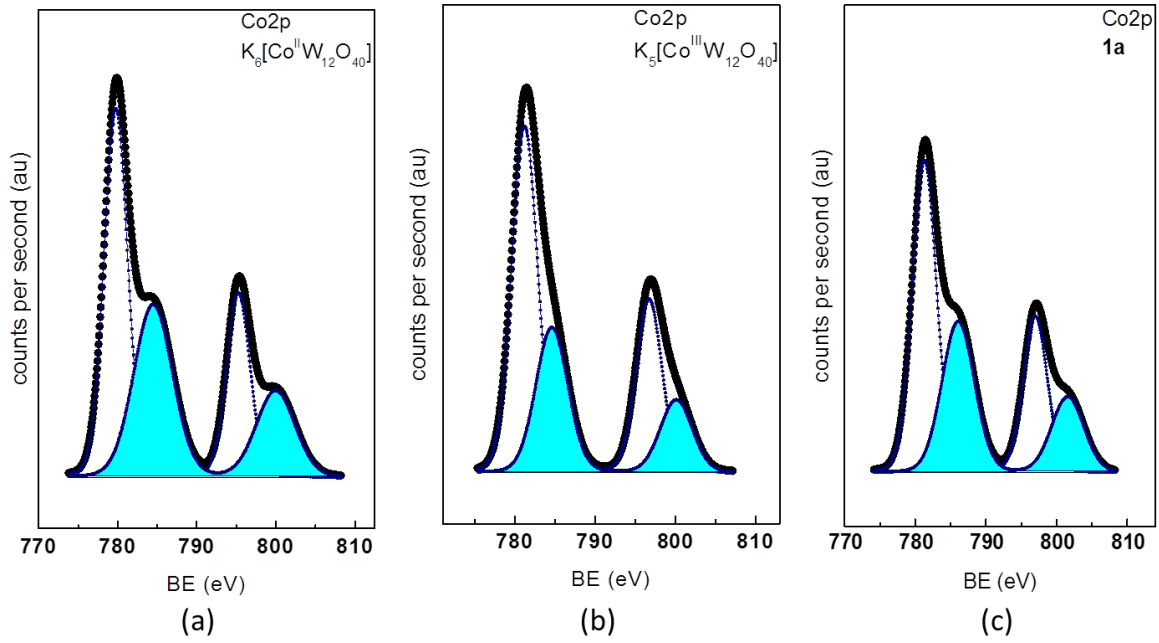

Fig. S13. XPS spectra of Co-containing samples: (a). $K_6[Co^{II}W_{12}O_{40}]$, (b). $K_5[Co^{III}W_{12}O_{40}]$ and (c). **1a**.

12. References

[1] C. Giménez-Saiz, J. R. Galán-Mascarós, S. Triki, E. Coronado, L. Ouahab, *Inorg.Chem.,* 1995, *34,* 524-526.

[2] CrysAlis PRO Software system, *version 1.171.35.15*; Agilent Technologies UK Ltd, Oxford, UK. (2013).

[3] G. M. Sheldrick, *Acta Crystallogr., Sect. A: Found. Adv.* 2008, *64*, 112-122.

[4] Q. Yin, J. M. Tan, C. Besson, Y. V. Geletii, D. G. Musaev, A. E. Kuznetsov, Z. Luo, K. I. Hardcastle, C. L. Hill, *Science,* 2010, *328,* 342-345.

[5] A. L. Nolan, C. C. Allen, R. C. Burns, D. C. Craig, G. A. Lawrance, *Aust.J.Chem.,* 2000, *53,* 59-66.

[6] I. D. Brown, D. Altermatt, *Acta Crystallogr. Sect. B,* 1985, *41,* 244-247.

[7] R. M. Wood, G. J. Palenik, *Inorg.Chem.,* 1998, *37,* 4149-4151.

[8] N. E. Brese, M. Okeeffe, *Acta Crystallogr. Sect. B,* 1991, *47,* 192-197.

[9] (a) N. Casañ-Pastor, J. Bas-Serra, E. Coronado, G. Pourroy, L. C. W. Baker, *J.Am.Chem.Soc.,* 1992, *114,* 10380-10383; (b) J. M. Clemente-Juan, H. Andres, M. Aebersold, J. J. Borrás-Almenar, E. Coronado, H. U. Güdel, H. Büttner, G. Kearly, *Inorg.Chem.,* 1997, *36,* 2244-2245; (c) H. Andres, J. M. Clemente-Juan, M. Aebersold, H. U. Güdel, E. Coronado, H. Büttner, G. Kearly, J. Melero, R. Burriel, *J.Am.Chem.Soc.,* 1999, *121,* 10028-10034; (d) H. Andres, J. M. Clemente-Juan, R. Basler, M. Aebersold, H. U. Güdel, J. J. Borrás-Almenar, A. Gaita, E. Coronado, H. Buttner, S. Janssen, *Inorg.Chem.,* 2001, *40,* 1943-1950; (e) J. M. Clemente-Juan, E. Coronado, A. Gaita-Ariño, C. Giménez-Saiz, G. Chaboussant, H. U. Güdel, R. Burriel, H. Mutka, *Chemistry-a European Journal,* 2002, *8,* 5701-5708; (f) J. M. Clemente-Juan, E. Coronado, A. Forment-Aliaga, J. R. Galán-Mascarós, C. Giménez-Saiz, C. J. Gómez-García, *Inorg.Chem.,* 2004, *43,* 2689-2694; (g) J. M. Clemente-Juan, E. Coronado, A. Gaita-Ariño, C. Giménez-Saiz, H. U. Güdel, A. Sieber, R. Bircher, H. Mutka, *Inorg.Chem.,* 2005, *44,* 3389-3395; (h) Y. Duan, J. M. Clemente-Juan, C. Giménez-Saiz, E. Coronado, *Inorg.Chem.,* 2016, *55,* 925-938.